BUTTERWORTH HEINEMANN

Natural convection in central microcavities of vertical, finned enclosures of very high aspect ratios

Ramón L. Frederick and Alvaro Valencia
Universidad de Chile, Departamento de Ingeniería Mecánica, Santiago, Chile

Natural convection in the central microcavities of vertical, finned cavities of very high aspect ratios were numerically investigated using a spacewise periodical approach. When equally spaced fins are located on both active walls (problem *b*), different circulation rates are found in two consecutive microcavities. The average Nusselt number in a region comprising two consecutive microcavities is higher than the one observed when the fins are attached to only one of the active walls (problem *a*). The dependence of microcavity circulation rates and heat transfer on Rayleigh number, dimensionless fin length, and microcavity aspect ratio is discussed. The limits of applicability of the spacewise periodical approach are also outlined.

Keywords: natural convection; finned cavities

Introduction

Natural convection in differentially heated cavities or channels with internal partitions has been studied extensively over the last few years. Kelkar and Patankar (1990) and Ciofalo and Karayiannis (1991) studied the effect of adding partitions to insulated cavity walls, while others have solved the problem with partitions added to the active walls (Meyer et al. 1982; Frederick 1989; Frederick and Valencia 1989; Scozia and Frederick 1991; Lin and Hsieh 1990). In addition, recent works dealing with inner bodies in natural convection channel flows have been published (Naylor and Tarasuk 1993). The main goal of most of these works was to determine the extent to which heat transfer rates can be modified by the presence of internal bodies that affect the flow pattern.

In confined spaces, two types of partitions have been considered. While the cases where partitions are attached to the passive, horizontal walls lead generally to heat transfer reductions, relative to the undivided cavity, the opposite trend is often observed in studies of the second kind (Meyer et al. 1982; Frederick 1989; Frederick and Valencia 1989; Scozia and Frederick 1991; Lin and Hsieh 1990). In square cavities, the effect of partitions on total heat transfer is moderate (Kelkar and Patankar 1990; Meyer et al. 1982; Frederick and Valencia 1989), because the partition does not change the circulation rates and modes very significantly. Moderate reductions are also found in slender cavities with baffles on insulated walls (Ciofalo and Karayiannis 1991). In slender cavities with multiple fins on the vertical active walls, however, very significant enhancements in heat transfer have been observed (Scozia and Frederick), caused by fin-generated flow recirculations that interact with a primary circulation, in a very complex succession of flow patterns.

Address reprint requests to Prof. Ramón L. Frederick, Dept. de Ingeniería Mecánica, Casilla 2777, Santiago, Chile.

Received 9 December 1993; accepted 9 December 1994

Int. J. Heat and Fluid Flow 16: 114–124, 1995

655 Avenue of the Americas, New York, NY 10010

In most applications, very high aspect ratios are used. The fundamental problem of natural convection in slender, differentially heated, undivided cavities has been treated in a number of excellent papers (e.g., Lee and Korpela 1983; Le Quéré 1990; Novak and Nowak 1993). It has been shown that, for most fluids at low Rayleigh numbers, the basic flow pattern consists of a single cell formed by two parallel flows of opposite directions with linear temperature profile across the cavity, except at the ends where the fluid turns. Transition to multicellular convection appears at higher Ra, leading to an increase in overall Nusselt number. Steady states are attained at Prandtl numbers up to approximately 12.5 (Le Quéré). When air ($Pr = 0.71$) is used as the test fluid, the multiple circulations arise as a result of the interaction of vertical flows of opposite directions in the presence of a vertical thermal stratification. As the aspect ratio is increased at a given Ra, the size of the cells tends to become uniform over most of the cavity height, with variations localized at or near the cavity ends. The stream function maps shown in Lee and Korpela, Le Quéré, and Novak and Nowak clearly show the existence of stagnation points located at the vertical ends of the cells.

If the tall cavity geometry is modified by adding fins to one of the vertical active walls, a primary circulation pattern, coupled with recirculations in the interfin spaces (microcavities) is observed (Scozia and Frederick 1991). Stagnation points, located near the fin tips, divide the primary circulation and the recirculations. Except for a narrow range of microcavity aspect ratios A in inclined cavities, flow structures tend to repeat themselves in successive microcavities, giving essentially identical flow patterns in all of them, except in some of the microcavities located at or near the cavity ends. This behavior, which clearly indicates a fin-determined flow pattern, was observed in Scozia and Frederick over wide ranges of the independent variables, except at very low microcavity aspect ratios (0.333, 0.25), where flow instabilities similar to those described in Lee and Korpela (1983), Le Quéré (1990) and Novak and Nowak (1993) were found on the unfinned side at high Ra.

SSDI 0142-727X/95/$10.00
SSDI 0142-727X(94)00021-4

It would be interesting to complement the study in Scozia and Frederick (1991) by treating the problem of natural convection in a tall vertical cavity with partitions attached to both active walls. In such a case, the fluid would be compelled to adopt an alternating direction flow pattern as it flows past the obstacles, and the heat transfer rates are bound to differ from those found in the case studied in Scozia and Frederick.

Several other issues addressed in Scozia and Frederick (1991) require further clarification. In that study, an overall aspect ratio of 20 was used. When dealing with cavities of very high aspect ratio, it is desirable to have means to evaluate the essential features of flow and heat transfer by using a restricted region of analysis in order to alleviate the computational burden. Following this line of thought, some attempts were made in Scozia and Frederick to obtain results using a spatially periodical approach. The results obtained using one microcavity only as a region of analysis showed flow patterns closely similar to those found in the central microcavities of a tall, divided cavity, as evidenced by the values of ψ_{max} obtained in both cases, which did not differ by more than 1 percent. However, for given values of the Rayleigh number, partition length, and microcavity aspect ratio A, the average Nusselt numbers Nu_{av} for one microcavity were always found to be lower than the overall Nusselt number Nu_{ov} computed for the whole height of a cavity of aspect ratio 20. At $Ra = 10^4$, Nu_{ov} exceeded Nu_{av} by only 0.5 percent at $A = 1$, but the deviation became as high as 5 percent at $A = 5$. This difference is caused by the higher heat transfer rates that occur at the cavity ends, where the fluid turns. The above results show that end effects on the overall heat transfer can be very important if the relationship between the microcavity and overall aspect ratios allows the existence of only few of the microcavities showing flow patterns similar to the central ones. Conversely, the difference between Nu_{ov} and Nu_{av} will be reduced with increases in the overall aspect ratio of the cavity, at a given microcavity aspect ratio.

Spatially periodic flow patterns have been also found to occur in forced, finned duct flows (Patankar et al. 1977; Choi and Amand 1993; Kelkar and Patankar 1987), in natural circulation duct flows (Lin and Hsieh 1990) and in confined, recirculating flows (Meyer et al. 1982). The spatial periodicity has been used as the basis of the numerical approach to the flow in some of these works.

In this work we study the laminar natural convection of air in the central microcavities of vertical enclosures with equally spaced baffles attached either to one of the active walls (problem *a*) or to both active walls (problem *b*). Contrary to the work in Scozia and Frederick (1991), emphasis now is placed on the detailed description of flow pattern in the central microcavities of a very high aspect ratio enclosure rather than on the flow in the entire cavity. It is assumed throughout that the relationship $A \ll A_o$ holds. Using the spacewise periodical assumption, solutions of the governing equations are obtained by using a solution domain whose height is equal to only one or two microcavities, according to the case studied. The local flow and heat transfer mechanisms, and parametric effects on the circulation and average Nusselt numbers for the region under study Nu_{av} are described. It must be remembered that Nu_{av} is *not* representative of the heat transfer over the whole height of a cavity, as shown above. Owing to the end effects, the relationship $Nu_{av} < Nu_{ov}$ always holds.

In forced convection, finned duct flows the applicability of the spacewise periodical approach is self-evident. This is not the case for the problems of natural convection in regions bounded by vertical active walls, where recirculation patterns can be generated either by the fins or by mechanisms such as the one described in Lee and Korpela (1983), Le Quéré (1990), and Novak and Nowak (1993). To evaluate the limits of applicability of the spacewise periodical approach, a considerable amount of work is devoted here to the detection of the limiting parameters for which the flow pattern changes from a fin-generated structure to a fin-independent, multicellular regime governed by an overall aspect ratio A_o.

Rayleigh numbers of 10^4 and 10^5, microcavity aspect ratios of 0.5–5, and dimensionless fin lengths of $l/L = 0.25$–0.75 are used. The thermal conductivity of the fins is taken equal to that of glass, which is reported to be about 28.6 times higher than the air thermal conductivity. In regard to the fin thickness δ, it has been found reasonable to keep the value δ/H constant, in order to have fin thicknesses representing a constant fraction of the microcavity height.

Formulation

The problem of natural convection in microcavities located at the midheight of a slender, vertical, air-filled enclosure is

Notation

A	microcavity aspect ratio (H/L)
A_o	overall aspect ratio of a slender enclosure
H	microcavity height
k	air thermal conductivity
k_f	fin thermal conductivity
L	cavity width
l	fin length
Nu_{av}	average Nusselt number for the region of analysis, based on L
Nu_{ov}	overall Nusselt number for an entire enclosure, based on L
p	dimensional pressure
P	dimensionless pressure ($pL^2/\rho\nu^2$)
Pr	Prandtl number (ν/α)
Q	dimensional heat flow
Ra	Rayleigh number [$g\beta\Delta TL^3/(\nu\alpha)$]
R_k	thermal conductivity ratio (k_f/k)
T	temperature
T_h, T_c	hot and cold wall temperatures
u, v	dimensional velocities in X and Y directions
U, V	dimensionless velocities ($U = uL/\nu$, $V = vL/\nu$)
x, y	dimensional coordinates
X, Y	dimensionless coordinates ($X = x/L$; $Y = y/L$)

Greek

α	thermal diffusivity
β	thermal expansion coefficient
Γ	generic dependent variable
ΔT	$T_h - T_c$
ΔX, ΔY	dimensionless grid spacings in the X and Y directions
δ	dimensional fin thickness
θ	dimensionless temperature ($(T - T_c)/\Delta T$)
ν	kinematic viscosity
ρ	density
Ψ	dimensional stream function
ψ	dimensionless stream function (Ψ/ν)
ψ_{max}	maximum dimensionless stream function
ψ_{st}	dimensionless stream function at the stagnation point

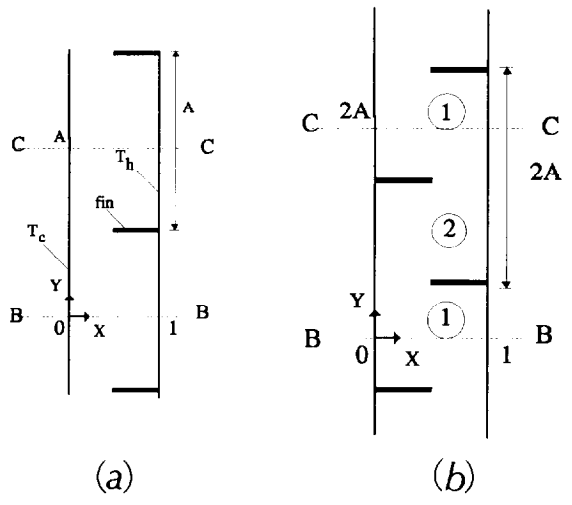

Figure 1 Physical model, region of analysis, coordinates, and their dimensionless values for problems (*a*) and (*b*) (Microcavities of types 1 and 2 are indicated by circled numbers)

formulated. The physical situation is shown in Figure 1. In problem (*a*) (Figure 1a), equally spaced fins are placed on the right-hand wall. The region of analysis for this problem is bounded by the horizontal lines *BB* and *CC* and the vertical walls of the enclosure in this figure. One fin is shown at the horizontal midplane of the region of analysis, whose height is equal to the microcavity height and to the fin spacing. The region of analysis is the upper and lower halves of two consecutive microcavities. In this way, it is easier to apply the boundary conditions that impose the vertical spacewise periodicity. The origin of coordinates is set at the bottom left corner of the region of analysis.

Figure 1b shows the physical situation for the case of fins located on both vertical walls (problem *b*). In this case, the height of the region of analysis (between lines *BB* and *CC* and the vertical walls), is equal to two times the microcavity height.

For both problems, the microcavity aspect ratio is defined as $A = H/L$, where H is the vertical distance between two consecutive fins. The left-hand wall is at a temperature T_c, while the right-hand one is at T_h, with $T_h > T_c$.

For an incompressible Boussinesq fluid, the two-dimensional (2-D), steady-state, laminar governing equations of continuity, X-momentum, Y-momentum and energy, in dimensionless form (Equations 1–4) are, respectively, as follows:

$$\frac{\partial U}{\partial X} + \frac{\partial V}{\partial Y} = 0 \tag{1}$$

$$U\frac{\partial U}{\partial X} + V\frac{\partial U}{\partial Y} = -\frac{\partial P}{\partial X} + \nabla^2 U \tag{2}$$

$$U\frac{\partial V}{\partial X} + V\frac{\partial V}{\partial Y} = -\frac{\partial P}{\partial Y} + (\mathrm{Ra}/\mathrm{Pr})\Theta + \nabla^2 V \tag{3}$$

$$U\frac{\partial \Theta}{\partial X} + V\frac{\partial \Theta}{\partial Y} = (1/\mathrm{Pr})\nabla^2\Theta \tag{4}$$

On the fin material, the velocities U and V are zero, so only the energy equation needs to be solved. The energy equation in a solid material in steady state takes the usual form:

$$\nabla^2\Theta = 0 \tag{5}$$

In both problems, the X boundary conditions are: $\Theta = 1$ and 0 at the hot ($X = 1$) and cold ($X = 0$) walls, respectively. $U = V = 0$ on all walls.

The Y boundary conditions that impose spacewise periodicity in the vertical direction for problem (*a*) are as follows:

$$\Gamma(X, 0) = \Gamma(X, A) \tag{6}$$

$$\frac{\partial \Gamma}{\partial Y}(X, 0) = \frac{\partial \Gamma}{\partial Y}(X, A) \tag{7}$$

where Γ is any of the dependent variables; namely, U, V, P, and Θ.

In problem (*b*), equally spaced fins are attached to both walls. A forced convection study in a geometry closely similar to that in Figure 1b (Kelkar and Patankar 1987) used only one microcavity as calculation domain. An inverted symmetry was found to occur in that case between two consecutive microcavities. In our problem, given the characteristics of buoyancy force, such a symmetry is not observed, as it is demonstrated below. Therefore, the region of analysis for problem (*b*), which must contain at least one fin attached to each active wall, will have the height of two microcavities ($2A$), as shown in Figure 1b. In this way, two types of microcavities can be defined: in those of type 1, the hot fin is on top and the cold one at the bottom. The opposite arrangement defines the microcavities of type 2. The Y boundary conditions are, therefore, written as follows:

$$\Gamma(X, 0) = \Gamma(X, 2A) \tag{8}$$

$$\frac{\partial \Gamma}{\partial Y}(X, 0) = \frac{\partial \Gamma}{\partial Y}(X, 2A) \tag{9}$$

as before, Γ stands for any of the dependent variables, namely U, V, P, and Θ.

The boundary conditions for the fins in both problems are expressed as follows. At the fin base, $\Theta(X = 0) = 0$ if the fin is located at the left-hand wall, while $\Theta(X = 1) = 1$ if the fin is located at the right-hand wall. The boundary condition at the fin tip expresses the continuity of heat flux through the interface: for a left-hand fin at $X = l/L$:

$$R_k\left[\frac{\partial \Theta}{\partial X}\right]_{\mathrm{fin}} = \left[\frac{\partial \Theta}{\partial X}\right]_{\mathrm{fluid}} \tag{10}$$

while for a right-hand fin at $X = 1 - l/L$:

$$\left[\frac{\partial \Theta}{\partial X}\right]_{\mathrm{fluid}} = R_k\left[\frac{\partial \Theta}{\partial X}\right]_{\mathrm{fin}} \tag{11}$$

In the last two equations, the left-hand members are evaluated at the left side of the fin tip. The Y boundary conditions for the fin are of the same nature as the preceding ones.

The flow and temperature fields are calculated from the governing equations in their primitive form (Equations 1–4). The stream function is obtained by solving the Poisson equation once a converged solution for the velocity field has been obtained.

Numerical method

The steady-state governing equations were iteratively solved by the SIMPLEC method. The code was tested against de Vahl-Davis (1983) benchmark solution for the problem of differentially heated square cavities, finding excellent agreement: using a grid of 41 × 41 points, the average wall Nusselt number obtained using our code differed by only 2.7 percent from the benchmark solution in de Vahl-Davis.

The numerical treatment of the fin–fluid interfaces can be made along the lines established by the boundary conditions

given in the formulation. However, the SIMPLEC method (Patankar 1980) and its enhancements allow a much more simpler treatment of conjugate problems of this kind.

According to the practice suggested in Patankar (1980), the temperature, pressure, and velocity fields are solved by using the same governing equations on the solid and fluid zones. In fact, the governing equations for the solid are the same as in the fluid except for the difference in thermophysical properties and the zero velocity field. A zero velocity field on the fin material is achieved by adding a source term of very high magnitude (10^{20}) to the right-hand side of Equations (2) and (3) in the control volumes where the fin is located. To achieve the thermal coupling between the solid and fluid zones, the diffusion coefficients in the discretized form of the energy equation are locally modified according to the harmonic-mean practice (Patankar), in order to account for the abrupt change of thermal conductivity from the fluid to the fin material.

Because the interest is now centered on the flow structure in the "generic" microcavity, no solutions for a complete cavity were run, and therefore, a very fine grid was used. Grids of 41 × 41 and 41 × 81 points were used for cases (*a*) and (*b*), respectively, in order to get the same resolution of flow and temperature fields in both cases. The X grid spacing was kept constant ($\Delta X = 0.025$), while the Y grid spacing ΔY was varied from 0.0125 at $A = 0.5$ to 0.125 at $A = 5$. The fin thickness was made to correspond to one control volume width in the Y direction ΔY.

To ensure the adequacy of the chosen grid, calibration runs were performed for case (*a*) with $A = 1$, $\mathrm{Ra} = 10^5$, $l/L = 0.75$, using grids of 41 × 41 and 81 × 81 points. With the finer grid, the fin thickness was of $2\Delta Y$. The values of ψ_{max} in these two runs differed by 1.38 percent, while the average Nusselt numbers on the fin-free walls differed by only 0.2 percent. This test proved two things: first, that the 41 × 41 grid gives sufficient accuracy for the study of flow and heat transfer characteristics of problem (*a*) with the code used; and second, that the treatment given to the fin boundary was able to give grid-independent results. It follows from the above reasoning that a 41 × 81 grid would be good enough for problem (*b*), as the grid spacings at a given A are the same as the ones used in the 41 × 41 grid of problem (*a*).

The averaging of Nusselt numbers over a finned wall is more difficult than averaging on a fin-free wall. The ability of the code to obtain such averages was tested as follows: comparing Nusselt numbers averaged on finned and unfinned walls in problem (*a*), differences of up to 13 percent were found. This difference is caused by the high thermal conductivity of the fin, which produces a sharp peak in local Nusselt number, which is difficult to integrate accurately. Although these differences were greatly reduced by using the 81 × 81 grid, it was decided to maintain the choice of a 41 × 41 grid (which was good enough for all other purposes) and to avoid inaccuracies in the integration by obtaining the average Nusselt numbers on the fin-free wall only.

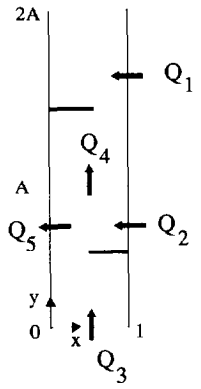

Figure 2 Heat flow contributions used in the calculation of Nu_{av} for the region of analysis in problem (*b*). The meaning of these contributions is given in the text

In case (*b*), the calculation of the finned wall average Nusselt number had to be made indirectly, because the presence of fins on both vertical walls of the region of analysis could not be avoided. The average Nusselt number over the hot wall from $Y = 0$ to $Y = 2A$ is $\mathrm{Nu}_{av} = Q/(2Ak\Delta T)$, where the total heat Q crossing the hot wall from $Y = 0$ to $Y = 2A$ is $Q = Q_1 + Q_2$ (see Figure 2 for details). Q_1 and Q_2 are the heat flows crossing the hot wall from $Y = A$ to $Y = 2A$ and from $Y = 0$ to $Y = A$, respectively. Whereas Q_1 is determined by direct integration of the Fourier local heat flow over the corresponding wall height, Q_2 is obtained from a heat balance over the lower half of the region depicted in Figure 2, written as $Q_2 = Q_4 + Q_5 - Q_3$. In this equation, Q_5 is the heat flow crossing the cold wall from $Y = 0$ to $Y = A$, while Q_3 and Q_4 are the conduction–convection heat flows crossing the horizontal lines at $Y = 0$ and $Y = A$, respectively. Therefore, $Q = Q_1 + Q_4 + Q_5 - Q_3$. It is

Table 1 Stream functions in problem (*a*)

$\mathrm{Ra} = 10^4$	$l/L = 0.25$		$l/L = 0.5$		$l/L = 0.75$	
A	ψ_{max}	ψ_{st}	ψ_{max}	ψ_{st}	ψ_{max}	ψ_{st}
0.5	14.535	14.528	3.842	3.689	0.876	0.345
1	17.354	17.278	8.082	4.222	6.189	0.335
2	23.126	13.452	15.677	3.708	14.177	0.265
5	30.076	14.057	24.768	3.425	24.034	0.217
$\mathrm{Ra} = 10^5$	$l/L = 0.25$		$l/L = 0.5$		$l/L = 0.75$	
A	ψ_{max}	ψ_{st}	ψ_{max}	ψ_{st}	ψ_{max}	ψ_{st}
0.5	—	—	33.707	33.117	7.166	3.694
1	—	—	37.917	26.605	18.858	3.765
2	—	—	60.648	20.958	30.308	2.345
5	—	—	67.480	11.143	55.233	1.243

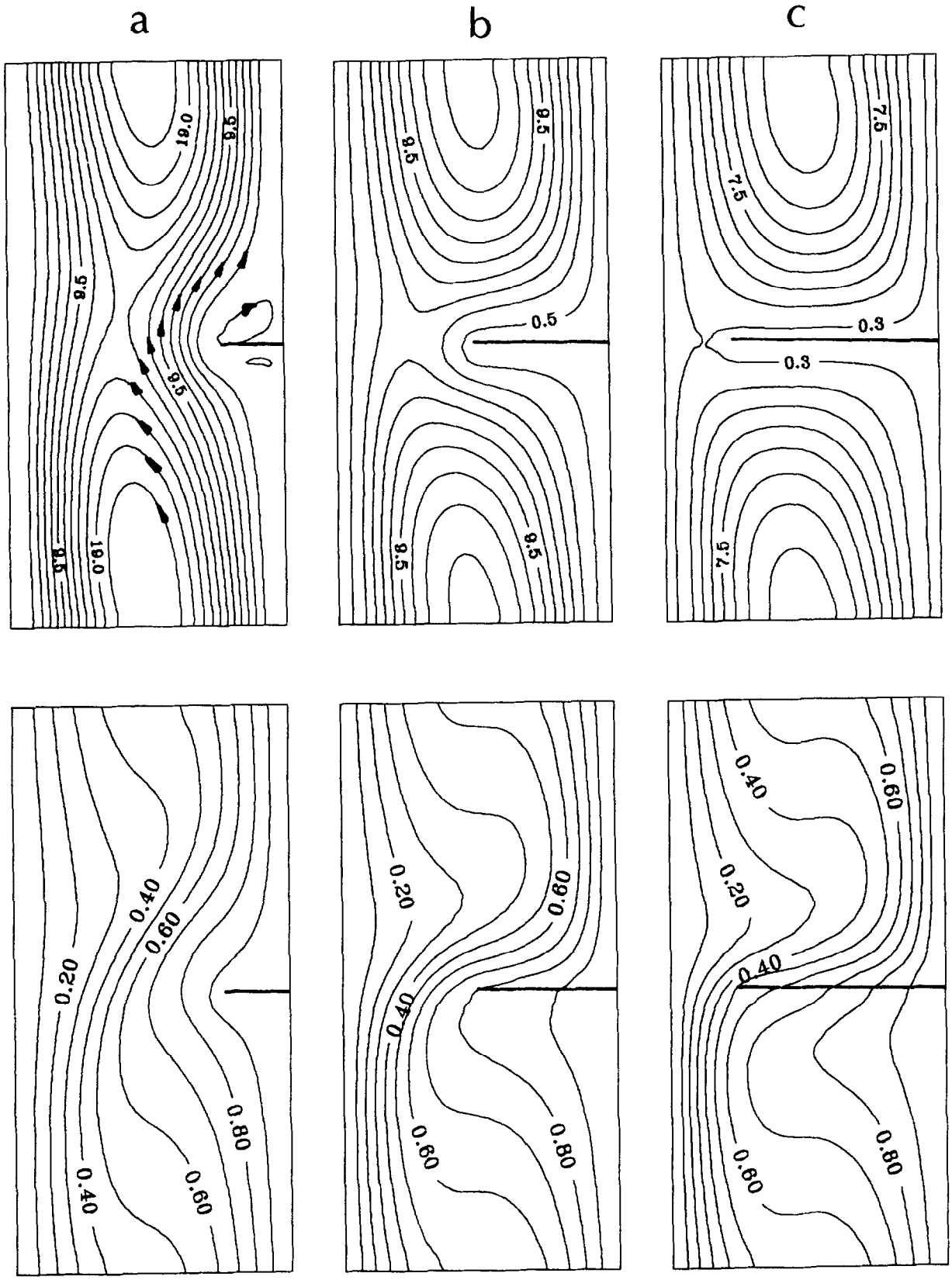

Figure 3 Stream function contours and isotherms for problem (*a*), Ra = 10^4, $A = 2$; a) $l/L = 0.25$: $-0.02 \leq \psi \leq 20.98$; b) $l/L = 0.5$: $0.5 \leq \psi \leq 15.20$; c) $l/L = 0.75$: $0.26 \leq \psi \leq 13.56$. (In this and in the following figures, the stream function contours of the primary circulation extend all along the region of analysis; ψ_{st} is located at the intersection of two branches of a contour so that any other contour for which $\psi > \psi_{st}$ will not cross the horizontal line at which the fin is located and belongs, therefore, to the recirculating stream; ψ_{max} is located approximately at the center of the recirculating stream; for values of ψ_{max} and ψ_{st}, see Table 1)

easily shown that Nu_{av} can be written as follows:

$$Nu_{av} = \frac{1}{2A}\left[\int_A^{2A}\left[\frac{\partial\Theta}{\partial X}\right]_{X=1} dY + \int_0^A \left[\frac{\partial\Theta}{\partial X}\right]_{X=0} dY + \int_0^1 \left[Pr\ V\Theta - \frac{\partial\Theta}{\partial Y}\right]_{Y=A} dX - \int_0^1 \left[Pr\ V\Theta - \frac{\partial\Theta}{\partial Y}\right]_{Y=0} dX\right]$$

This formula was used in all calculations of Nu_{av} of case (*b*).

The accuracy of the results of this work can be estimated to be better than that obtained in Scozia and Frederick (1991), in which coarser grids were used in the cases treated by means of the spacewise periodical approach.

Results and discussion

The details of flow structure inside the microcavities are described here. Table 1 shows important values of dependent variables for the ranges of parameters investigated in problem (*a*). Positive values of stream function correspond to counterclockwise circulation. Dashes in the tables indicate the situations in which the spacewise periodical approach is not applicable. The flow patterns and temperature distributions can be seen in Figures 3–5. In these figures, horizontal boundaries are drawn to represent clearly the region of analysis; however, obviously the flow crosses these boundaries. In all contour plots, equally spaced lines are shown, and the stream functions plotted do not include the value $\psi = 0$. As already noted in Scozia and Frederick (1991), the flow structure (Figure 3) consists of: (1) a primary circulation, of upward and downward direction near the hot and cold walls respectively; and (2) recirculations in the microcavities. ψ_{st} is the value of stream function at the stagnation point, located in the vicinity of the fin tip, where the flow is divided into these two circulations. The value of ψ_{st} represents the flow rate of the primary circulation, while ψ_{max} gives the total circulation rate, whose value is located approximately at the microcavity center in the cases shown in Figure 3. For smaller aspect ratios, the point of maximum stream function is displaced to the left. $\psi_{max} - \psi_{st}$ is the flow rate of the recirculating stream.

The relative strengths of the primary circulation and recirculation depend on Ra, on the aspect ratio of the microcavities, and on the fin length. The buoyancy force exerted on the fluid is opposed by the drag on the microcavity walls and by the resistance caused by the flow contraction, resulting in the different values of stream function given for primary circulation and recirculation.

In all the range of independent parameters covered in this study, at a given Rayleigh number (Table 1), total circulation increases significantly with A for all the partition lengths investigated. The effect of l/L on ψ_{max} is also significant, especially at $Ra = 10^5$. The primary circulation, measured by ψ_{st}, remains fairly constant to variations of A for a given l/L, except at $Ra = 10^5$, where a consistent decrease in primary circulation with increases in A is noticed. The recirculation rate also grows significantly with A. Except for the cases in which short partition lengths and small aspect ratios are involved, the intensity of the recirculation greatly exceeds that of the primary circulation. The physical reasons for this behavior, which is closely similar to that found in a cavity of an overall aspect ratio of 20, were explained in detail in Scozia and Frederick (1991) and are not repeated here.

Figures 3–5 show also the temperature distributions. Significant temperature distortion, caused by the recirculating flow, is observed inside the microcavities. This distortion is more pronounced at higher fin lengths, where the recirculation flow has a significantly higher intensity than the primary circulation.

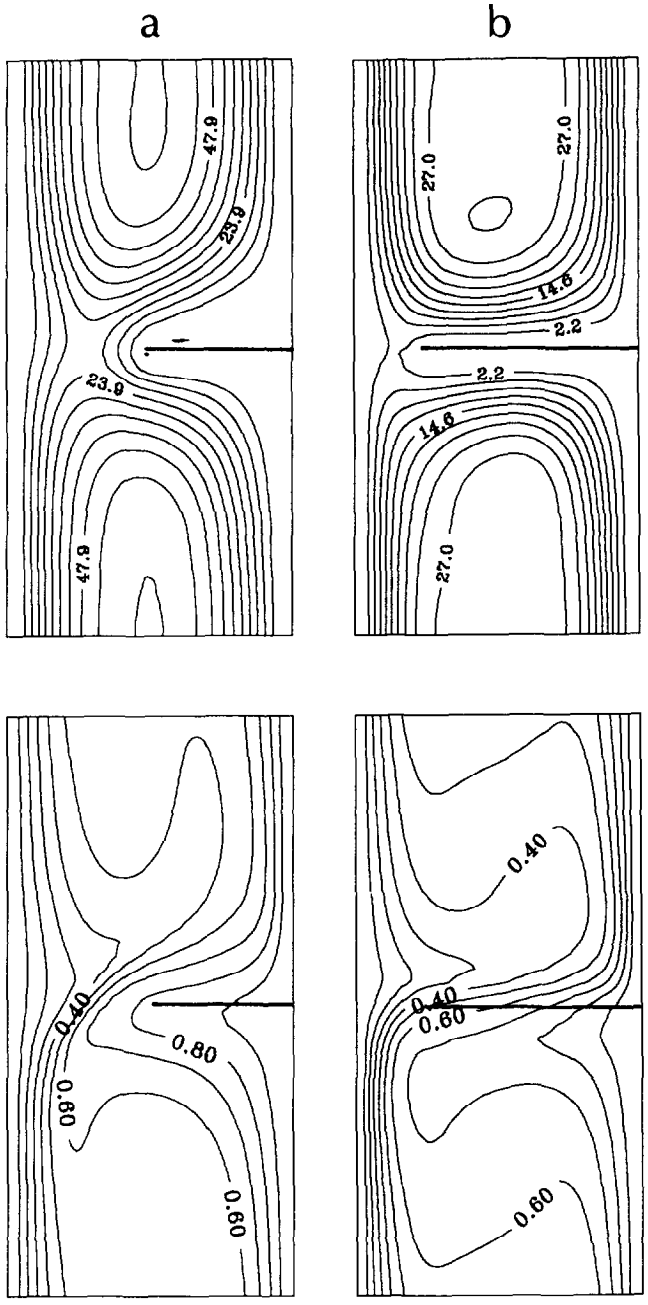

Figure 4 Stream function contours and isotherms for problem (*a*), $Ra = 10^5$, $A = 2$; a) $l/L = 0.5$: $-0.14 \le \psi \le 59.9$; b) $l/L = 0.75$: $2.2 \le \psi \le 31.0$

At $Ra = 10^4$ and $l/L = 0.5$, the results given by Scozia and Frederick (1991) for a cavity with an overall aspect ratio of 20, showed that the recirculations are always related to the presence of the fins (one recirculation per microcavity). This was also observed in that work, even at microcavity aspect ratios as low as 0.25, where the flow in the unobstructed side was almost completely vertical and showed conductive temperature profiles. The same happened at $l/L = 0.75$ and 0.25, at least up to $A = 0.5$. However, at $Ra = 10^5$, multiple circulations appeared in the unobstructed side, at A values of

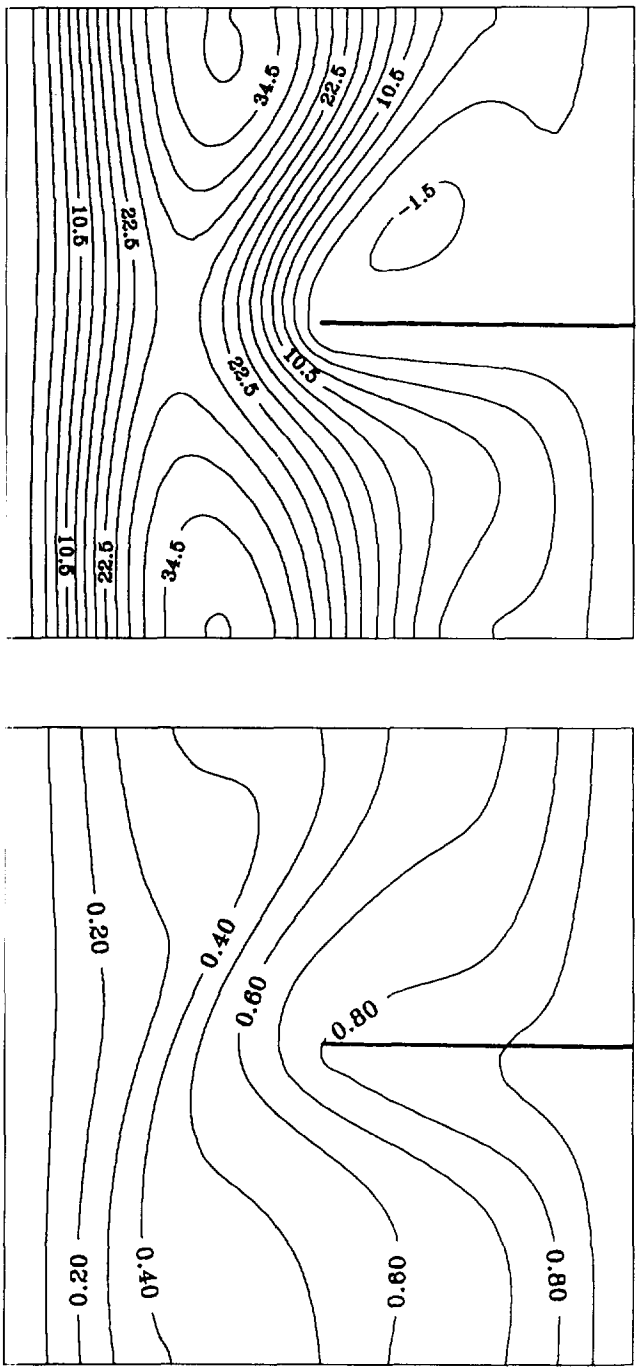

Figure 5 Stream function contours and isotherms for problem (*a*), Ra = 10^5, $A = 1$, $l/L = 0.5$: $-1.50 \leq \psi \leq 37.50$

0.333 and 0.25. These multiple circulations, which are not associated to any of the microcavities, were similar to those described by Lee and Korpela (1983), which arise from the interaction of opposing vertical flows in the presence of vertical temperature stratification.

In the present work, no recirculations of the type described in Lee and Korpela (1983) were observed at any values of A and Ra at $l/L = 0.75$ and 0.5, suggesting that these cases correspond also to a fin-determined flow pattern. This behavior is also observed at $l/L = 0.25$ when Ra = 10^4. In the cases for $l/L = 0.25$ and Ra = 10^5, there arises the necessity of judging whether the observed recirculations are fin-generated, or correspond sometimes to those described by Lee and Korpela. The region of analysis used in the present work does not allow us to check this directly. However, the following reasoning gives us criteria to settle this point.

Numerical results were obtained for Ra = 10^5, $l/L = 0.25$, and $A = 0.5 - 1$, (not shown in figures). In these conditions, the flow was predominantly vertical and no fin-generated recirculations were apparent. Secondary circulations of the type observed in an undivided tall cavity at lower Rayleigh numbers appear, although displaced to the left of the vertical axis. The temperature profile is essentially conductive. Moreover, the calculations for $A = 5$ did not converge at all. These facts show us that these cases are not tractable by the spacewise-periodic approach. For $A = 2$, the flow pattern was found to be similar to the typical fin-generated one. However, the previous considerations for higher and lower aspect ratios cast doubt on the observed flow pattern $A = 2$, so the results for Ra = 10^5, $l/L = 0.25$ will be discarded altogether.

In several cases, a secondary loop of retrograde circulation sense relative to the main flow is seen to appear above the fin (see Figures 3a and 5). Retrograde circulations occur when the fluid attains high levels of vertical velocity at the cross section between the cold wall and the fin. The fluid that ascends within a microcavity is diverted to the left by the partition. As it flows upward past the fin, the high velocity level reached in the contraction causes a separation of the fluid from the fin, which acts as a backstep, producing a circulation of opposite sense to the main one. Of all the cases analyzed for Ra = 10^4, reverse circulation is very significant at $l/L = 0.25$ (Figure 3a), because at this fin length the recirculating flow is weak, and relatively high vertical velocity levels are obtained. For Ra = 10^5, reverse circulation was also found at $l/L = 0.5$ and 0.75, because of the higher buoyancy force levels associated with this value of Ra, which tend to generate high vertical velocities, even in the presence of long fins. However, the order of magnitude of the retrograde circulation is too small for these circulations to be seen in Figures 4a and b.

Flow patterns in problem (*b*)

In this case (Figures 6 and 7) the most frequent flow regime consists, as before, of one recirculation flow established in each microcavity, and a primary circulation, with a stagnation point dividing the two circulations. The stagnation point is typically located in the vicinity of the fin tip. For some parameter combinations, however, (low aspect ratios and short fin lengths, $A = 0.5$, $l/L = 0.5$ and $A = 1$, $l/L = 0.25$), this flow pattern breaks up (Figure 8), and a second flow regime appears, consisting of a main circulation combined with a series of recirculations akin to those found in an undivided slender cavity, as described by Lee and Korpela (1983). The fact that these recirculation loops (Figure 8) are not restricted to the inside of any of the microcavities, but they are able to extend from one microcavity to another, with stagnation points far removed from the fin tips, suggests that these loops are not directly caused by the presence of the fins.

As shown by Lee and Korpela (1983) the multicellular convection in an undivided slender cavity is governed by Rayleigh number, Prandtl number, and overall aspect ratio. The latter dependence suggests that, in a finned cavity, we cannot ensure that a multicellular convection of this type is correctly described unless we use the entire enclosure as a region of analysis. In the case shown in Figure 8, the spatially periodical character imposed to the flow results in a solution which, in spite of sharing some of the characteristics of the multicellular convection described by Lee and Korpela, does not necessarily represent the correct flow structure for a finned cavity of very high aspect ratio. Such a regime, therefore, is not

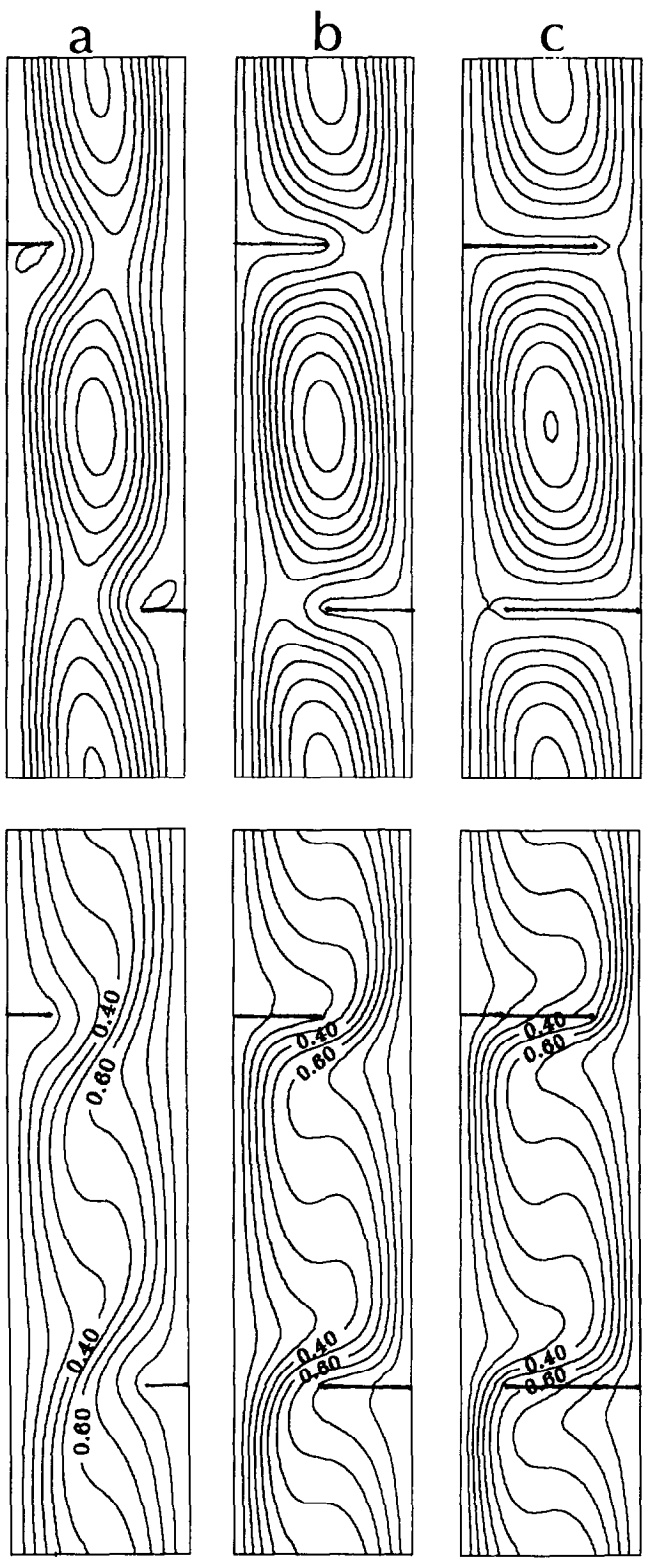

Figure 6 Stream function contours and isotherms for problem (*b*), $Ra = 10^4$, $A = 2$; a) $l/L = 0.25$: $-0.04 \leq \psi \leq 25.0$; b) $l/L = 0.5$: $0.3 \leq \psi \leq 17.1$; c) $l/L = 0.75$: $0.3 \leq \psi \leq 16.3$

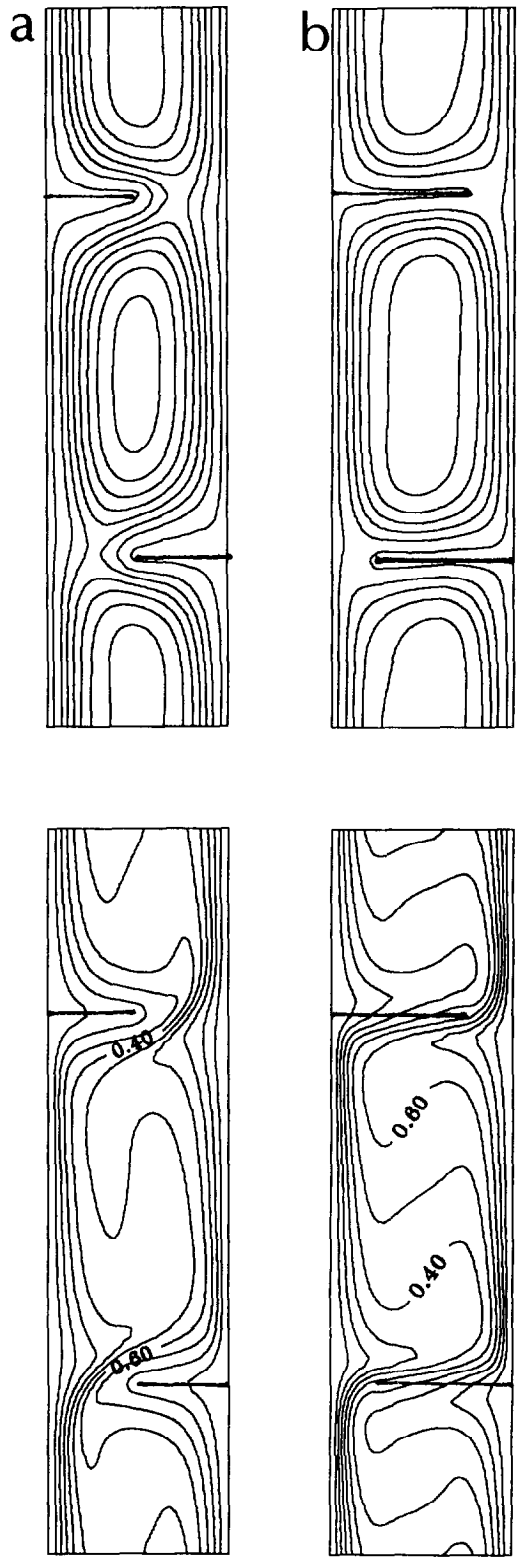

Figure 7 Stream function contours and isotherms for problem (*b*), $Ra = 10^5$, $A = 2$; a) $l/L = 0.5$: $1.0 \leq \psi \leq 60.0$; b) $l/L = 0.75$: $0.8 \leq \psi \leq 32.0$

described in this work, although the parameters bounding the two regimes can be given.

The range of parameters for which fin-generated recirculations are observed, is limited to values of $l/L = 0.75$ or higher, at both Rayleigh numbers investigated. For $Ra = 10^4$, this regime occurs at $A \geq 1$ when $l/L = 0.5$ and at $A \geq 2$ when $l/L = 0.25$. For $Ra = 10^5$, the regime of fin-generated recirculations does not occur at all at $l/L = 0.25$, and it appears only at $A \geq 2$ when $l/L = 0.5$.

In the regime of fin-generated recirculations, a major difference is observed in case (*b*) relative to (*a*). Whereas in (*a*) we find equal values of ψ_{max} in all microcavities, in case (*b*), the

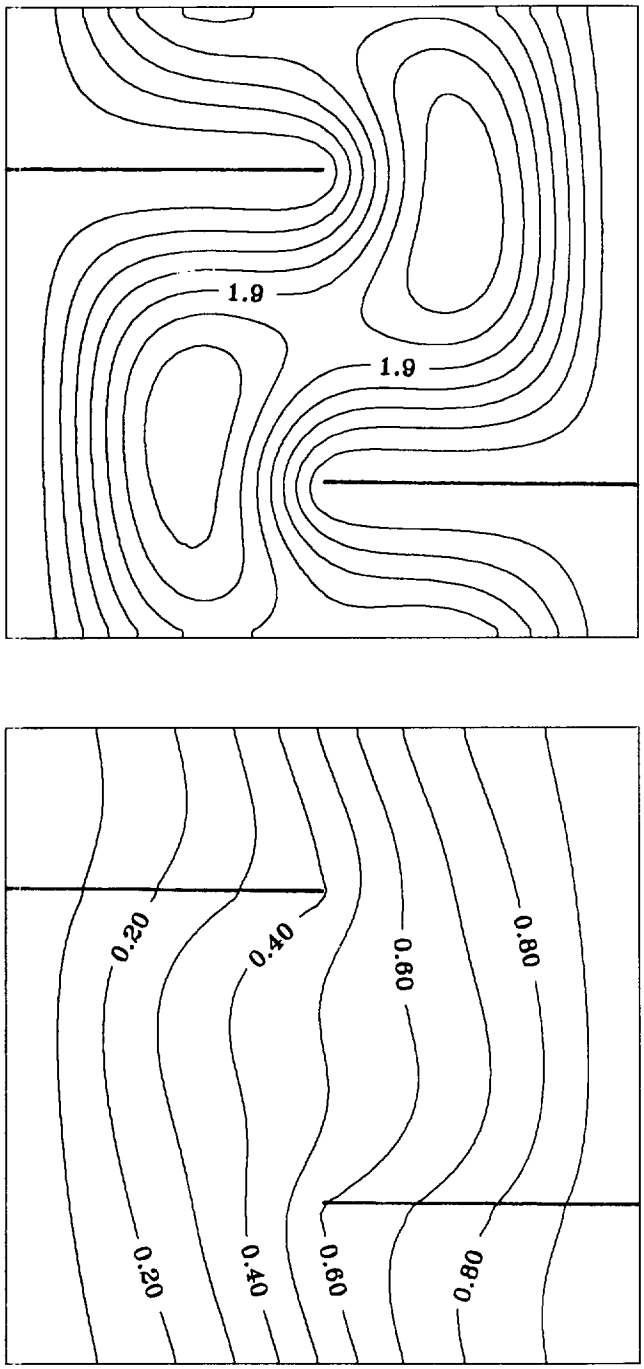

Figure 8 Stream function contours and isotherms for problem (*b*), Ra = 10^4, $A = 0.5$, $l/L = 0.5$: $0.3 \leq \psi \leq 3.0$

value of ψ_{max} is higher in microcavities of type 2 (hot fin at the bottom) than in microcavities of type 1 (e.g., in the case $A = 1$, $l/L = 0.5$, Ra = 10^4, values of ψ_{max} of 10.450 and 8.464 are found in microcavities of types 2 and 1, respectively—the value of ψ_{max} in problem (*a*) at the same independent parameters was 8.082). In this example, the circulation in both microcavities increases with respect to case (*a*), with a greater increase in the cavity of type 2. More frequently, however, the circulations in cavities 1 and 2 decrease and increase, respectively, with reference to the one in case (*a*). When the fins are long and the aspect ratios small, this behavior is more notorious (see Tables 1 and 2 for comparison) and has an impact on heat transfer, as will be seen later.

The different flow behavior in two consecutive microcavities, clearly seen in Figures 6 and 7, and Table 2, is explained as follows: The hot and cold streams that enter a microcavity of type 2 have been accelerated by wall buoyancy over unobstructed vertical lengths of $2A$ in neighboring microcavities. Both streams are diverted and further accelerated in the contraction. The collision of these two streams generates high rates of recirculation in cavities of type 2. Conversely, the entrance of hot and cold streams into a cavity of type 1 is located at its fin-free sides, and, therefore, these streams are not subject to contractions or changes of direction as they enter. The collision of the two streams entering a microcavity of type 1 is, therefore, weaker and does not generate a recirculation flow as intense as that found in an adjacent microcavity of type 2. As the hot and cold streams flow up and down within the microcavity 1, they are further accelerated by wall buoyancy until they reach their respective microcavities of type 2.

A second fact that partly explains the different circulations in two consecutive microcavities is the existence of Bénard effects. Microcavities of type 2 have a hot fin at the bottom and a cold one on top. The opposite occurs in microcavities of type 1. It is, therefore, reasonable to expect circulation to be assisted and opposed by these effects in microcavities of types 2 and 1, respectively.

The difference in recirculation rates between two consecutive microcavities, as explained above, is a direct consequence of the fact that these recirculations are caused by the presence of the fins. Cases in which this difference is not observed are likely to correspond, therefore, to multicellular convection governed by the overall aspect ratio.

The fact that in problem (*b*) there a fewer cases tractable by means of the spacewise periodic approach, relative to problem (*a*) can be explained as follows. In problem (*a*), there is a marked asymmetry of the flow with respect to the vertical axis of the enclosure. Even very short obstacles can deeply modify the flow pattern relative to that found in an undivided cavity, because they hinder the access of the fluid to one of the active walls. As seen in Figures 6 and 7, the more symmetrical positioning of the obstacles in problem (*b*) in relation to the vertical axis, has the result of inducing an alternating direction in both the upward and downward flows, more similar to the movement they would take in an undivided enclosure. When the fins are short enough, they represent only a slight source of distortion for the flow, whose pattern will, therefore, be essentially determined by the overall aspect ratio of the enclosure at a given Rayleigh number.

In some cases, retrograde loops are seen in microcavities of type 2, above the hot fin and below the cold one (Figure 6a). As before, these loops result from the high vertical velocities attained by the hot fluid in front of the hot fin (and by the cold fluid in front of the cold one). When the flow restriction is too severe ($l/L = 0.5$ and 0.75) no retrograde circulation is observed.

Heat transfer

The average Nusselt numbers in the region of analysis Nu_{av}, for problems (*a*) and (*b*) are given in Table 3 as a function of A and l/L for two Rayleigh numbers. In problem (*a*), longer partitions always lead to higher heat transfer rates, because of the predominance of recirculation over primary circulation. In most cases, it is seen that a maximum in Nu_{av} occurs at $A = 2$, with a slow decrease as A is increased. An exception occurs at Ra = 10^5, with partitions of length 0.5. In this case, the maximum heat transfer seems to be located at aspect ratios higher than 5. At Ra = 10^4, the heat transfer, as measured by Nu_{av}, is seen to be enhanced at least by 50 percent relative to

Table 2 Maximum stream functions in microcavities 1 and 2, problem (*b*)

$Ra = 10^4$	$l/L = 0.25$		$l/L = 0.5$		$l/L = 0.75$	
A	ψ_{max1}	ψ_{max2}	ψ_{max1}	ψ_{max2}	ψ_{max1}	ψ_{max2}
0.5	—	—	—	—	0.682	2.115
1	—	—	8.464	10.450	5.667	9.554
2	23.794	25.006	15.268	17.556	13.121	16.408
5	30.143	30.527	24.312	25.585	23.156	25.146
$Ra = 10^5$	$l/L = 0.25$		$l/L = 0.5$		$l/L = 0.75$	
A	ψ_{max1}	ψ_{max2}	ψ_{max1}	ψ_{max2}	ψ_{max1}	ψ_{max2}
0.5	—	—	—	—	6.470	9.468
1	—	—	—	—	16.836	22.304
2	—	—	52.301	61.000	26.855	33.409
5	—	—	59.622	68.993	50.199	59.544

the results given by Lee and Korpela (1983) for an infinite, undivided enclosure, in which the end effects are not significant.

It is interesting to note that most of the published heat transfer results for unfinned, high aspect ratio cavities refer to Rayleigh numbers not exceeding 30,000. Nusselt number results for undivided cavities of very high aspect ratios at $Ra = 10^5$ are not presently available. However, from information in Scozia and Frederick (1991), for an overall aspect ratio of 20, $Nu_{ov} = 2.888$. Heat transfer enhancements of up to 33 percent with respect to this value were obtained in this work. Taking into account that the Nusselt number results reported here correspond to the central microcavities of a high aspect ratio cavity, the overall heat transfer enhancement caused by the fins would be even higher if results for an entire finned cavity (including end effects) were compared with the value of Nu_{ov} given above.

The locally averaged Nusselt numbers of problem (*b*) can be compared with those of problem (*a*) only in the cases for which in both problems fin-generated recirculations are observed (Table 3). The values of Nu_{av} in problem (*b*) are consistently higher than those in (*a*) at the same values of the independent parameters (Ra, A, and l/L). The differences in Nusselt numbers are more notorious at lower microcavity aspect ratios, where increases of up to 23 percent were found in case (*b*) relative to (*a*). The differences become smaller at higher A: for microcavities of aspect ratios 2 and 5, the Nusselt number results are essentially equal for both problems, with differences that are within the range of accuracy of the determination of Nu_{av}.

By examining Tables 1–3, it can be seen that the increase in Nu_{av} in problem (*b*) relative to (*a*), when significant, occurs when the intensity of circulation in microcavities of type 2 in problem (*b*) increases very markedly with respect to the circulation in problem (*a*), and this increase is accompanied by a much smaller decrease (or no decrease at all) in circulation in cavity 1 with respect to the value in problem (*a*). At high aspect ratios (2–5), the total circulations in cavities of both types take values whose absolute differences with respect to the ψ_{max} of problem (*a*) are very similar between each other. The resulting average heat transfer (Nu_{av}) is, therefore, not significantly different from that observed in problem (*b*) at the same values of the independent parameters.

Conclusions

Natural convection in the central microcavities of finned, differentially heated, very tall cavities containing air was investigated. The spacewise periodical approach was used to determine flow and temperature distributions in the region of analysis. It was found that the results obtained using this approach are valid if and when the following three conditions

Table 3 Average Nusselt numbers in problem (*a*) and (*b*) at two Rayleigh numbers

$Ra = 10^4$	$l/L = 0.25$		$l/L = 0.5$		$l/L = 0.75$	
A	*a*	*b*	*a*	*b*	*a*	*b*
0.5	1.086	—	1.216	—	1.409	1.513
1	1.096	—	1.562	1.677	1.916	2.069
2	1.332	1.383	1.916	1.969	2.260	2.297
5	1.313	1.330	1.790	1.803	2.028	2.036
$Ra = 10^5$	$l/L = 0.25$		$l/L = 0.5$		$l/L = 0.75$	
A	*a*	*b*	*a*	*b*	*a*	*b*
0.5	—	—	1.270	—	2.124	2.616
1	—	—	1.650	—	3.582	3.677
2	—	—	2.780	2.825	3.843	3.877
5	—	—	3.085	3.155	3.630	3.628

are met. First, one recirculation loop per microcavity is obtained. Second, stagnation points located in the intermediate vicinity of the fin tips are found. Third, if fins are located on both active walls, the flow characteristics on two consecutive microcavities are different.

While in problem (*a*) equal flow structures are seen in all microcavities, in problem (*b*) the circulation intensity is higher in the microcavities with a hot fin at the bottom. This difference, caused by the different entry conditions in consecutive microcavities and by Bénard effects, is the cause of the moderate heat transfer increase observed in case (*b*) with respect to (*a*). This increase is only important for microcavity aspect ratios below 2. The heat transfer is also enhanced with respect to the case of undivided, high aspect ratio cavities. This conclusion is obtained indirectly, because no results for an entire finned cavity of high overall aspect ratio were obtained in this work.

References

Choi, J. M. and Anand, N. K. 1993. Heat transfer in a serpentine channel with a series of right angle turns. *Num. Heat Transfer*, **23**, 189–210

Ciofalo, M. and Karayiannis, T. G. 1991. Natural convection heat transfer in a partially—or completely—partitioned vertical rectangular enclosure. *Int. J. Heat Mass Transfer*, **34**, 167–179

de Vahl-Davis, G. 1983. Natural convection of air in a square cavity: a benchmark numerical solution. *Int. J. Num. Meth. Fluids*, **3**, 249–264

Frederick, R. L. 1989. Natural convection in an inclined square enclosure with a partition attached to its cold wall. *Int. J. Heat Mass Transfer*, **32**, 87–94

Frederick, R. L. and Valencia, A. 1989. Heat transfer in a square cavity with a conducting partition on its hot wall. *Int. Commun. Heat Mass Transfer*, **16**, 347–354

Kelkar, K. M. and Patankar, S. V. 1987. Numerical prediction of flow and heat transfer in a parallel plate channel with staggered fins. *J. Heat Transfer*, **109**, 25–30

Kelkar, K. M. and Patankar, S. V. 1990. Numerical prediction of natural convection in square partitioned enclosures. *Num. Heat Transfer*, **17**, 269–285

Lee, Y. and Korpela, S. A. 1983. Multicellular natural convection in a vertical slot. *J. Fluid Mech.*, **126**, 91–121.

Le Quéré, P. A. 1990. A note on multiple and unsteady solutions in two-dimensional convection in a tall cavity. *J. Heat Transfer*, **112**, 965–974

Lin, T. Y. and Hsieh, S. S. 1990. Natural convection of opposing/assisting flows in vertical channels with asymmetrically discrete heated ribs. *Int. J. Heat Mass Transfer*, **33**, 2295–2309

Meyer, B. A., Mitchell, J. W. and El-Wakil, M. M. 1982. The effect of thermal wall properties on natural convection in inclined rectangular cells. *J. Heat Transfer*, **104**, 111–117

Naylor, D. and Tarasuk, J. D. 1993. Natural convective heat transfer in a divided vertical channel: part I—numerical study. *J. Heat Transfer*, **115**, 377–387

Novak, M. H. and Nowak, E. S. 1993. Natural convection heat transfer in slender window cavities. *J. Heat Transfer*, **115**, 476–479

Patankar, S. V. 1980. *Numerical Heat Transfer and Fluid Flow*, Hemisphere/McGraw-Hill, Washington, 149

Patankar, S. V., Liu, C. H. and Sparrow, E. M. 1977. Fully developed flow and heat transfer in ducts having streamwise periodic variations of cross sectional area. *J. Heat Transfer*, **99**, 180–186

Scozia, R. and Frederick, R. L. 1991. Natural convection in slender cavities with multiple fins attached to an active wall. *Num. Heat Transfer*, **20**, 127–158